PCCP

Accepted Manuscript

ROYAL SOCIETY OF CHEMISTRY

www.rsc.org/pccp

Magnetic Susceptibility as a Direct Measure of Oxidation State in $LiFePO_4$ Batteries and Cyclic Water Gas Shift Reactors

Thomas Kadyk[a,*], Michael Eikerling[a]

a: Simon Fraser University, Department of Chemistry,
8888 University Drive, Burnaby, BC, V5A 1S6, Canada
*: Corresponding author. Email: tkadyk@sfu.ca, tel.: +1 778 782 3699

June 2015

Abstract

The possibility of correlating the magnetic susceptibility to the oxidation state of the porous active mass in a chemical or electrochemical reactor was analyzed. The magnetic permeability was calculated using a hierarchical model of the reactor. This model was applied to two practical examples: $LiFePO_4$ batteries, in which the oxidation state corresponds with the state-of-charge, and cyclic water gas shift reactors, in which the oxidation state corresponds to the depletion of the catalyst. In $LiFePO_4$ batteries phase separation of the lithiated and delithiated phases in the $LiFePO_4$ particles in the positive electrode gives rise to a hysteresis effect, i.e. the magnetic permeability depends on the history of the electrode. During fast charge or discharge, non-uniform lithium distributionin the electrode decreases the hysteresis effect. However, the overall sensitivity of the magnetic response to the state-of-charge lies in the range of 0.03%, which makes practical measurement challenging. In cyclic water gas shift reactors, the sensitivity is 4 orders of magnitude higher and without phase separation, no hysteresis occurs. This shows that the method is suitable for such reactors, in which large changes of the magnetic permeability of the active material occurs.

Keywords: lithium ion battery, water gas shift, magnetic permeability, susceptibility

1 Introduction

When atoms change their oxidation state, their magnetic moment changes. In some cases, this can lead to significant changes in the magnetic properties of a material. One example is iron, which changes its ferromagnetic nature when it is oxidized into paramagnetic FeO (i.e. iron(II) oxide). Further oxidation to Fe_3O_4 (iron(II,III) oxide) makes the material ferrimagnetic and finally Fe_2O_3 (iron(III) oxide) is again ferromagnetic [1]. This opens up the possibility to determine the oxidation state of the material via measurement of its magnetic susceptibility. This work attempts to explore this principle in two important practical example systems of chemical engineering: lithium ion phosphate ($LiFePO_4$) batteries and cyclic water gas shift reactors (CWGSR).

In CWGSR, the above mentioned transition from iron to iron oxide (usually to the FeO or Fe_3O_4 stage) is used as an intermediate oxygen storage for the water-gas-shift reaction ($CO + H_2O \leftrightarrow CO_2 + H_2$) used for hydrogen production [2–4]. The oxidation state of the reactor bed corresponds to the depletion of the catalyst, which is an important information for the operation of the reactor: when the catalyst is depleted, the reactor needs to be switched from an oxidation cycle to the reduction cycle in order to restore the catalyst. Ideally, the cycling should occur before the catalyst is completely depleted in order to avoid a breakthrough of the reactant gases.

In $LiFePO_4$ batteries, charges are stored in the negative electrode in the form of intercalated lithium. Upon charge, lithium deintercalates, which changes the oxidation state of iron from Fe^{2+} in $LiFePO_4$ to Fe^{3+} in delithiated $FePO_4$ (see Appendix A). Thus, the oxidation state is directly linked

to lithium content and state of charge of the battery.

The determination of the state of charge (SOC) of the battery is a major problem for battery management [5, 6]. On the one hand, the SOC is important information for the user in order to estimate the remaining working time of the device. It is an important psychological factor for which the term range anxiety has been coined in the context of electric vehicles. On the other hand, the knowledge of the SOC is important for the management of the battery, since many systems are sensitive to deep discharge or overcharge. These states of extremely high or too low SOC can cause irreversible damage to the battery [7].

Current strategies for determining the SOC (for a review, see e.g. [5, 6]) often suffer drawbacks [5, 6]: discharge tests are not applicable online; Coulomb counting needs continuous re-calibration and is sensitive to side reactions; measurement of OCV or EMF need long rest times before they can be applied; impedance spectroscopy is cost intensive and temperature sensitive; artificial neural networks need intensive training with a similar battery; Kalman filters need large computing capacities, a suitable battery model and determination of initial parameters. Therefore, an alternative, direct measure of SOC would be desireable.

One aim of the current work is to assess whether the change of the magnetic properties of a lithium ion battery during charge and discharge can be used to determine the SOC. A prominent method in literature of using the magnetic properties for the investigation of lithium ion batteries is nuclear magnetic resonance (NMR) spectroscopy. With NMR, interfacial storage mechanisms of lithium in RuO_2 [8], silicon [9] and hard carbon elec-

trodes [10, 11] were investigated. NMR was successfully used to investigate the local structure [12, 13] and the dynamics of lithium [12, 14] in battery electrodes. It was used to analyse the formation of microstructural lithium over the lifetime of the battery [13, 15] and the limited cyclability of Li-O_2 batteries [16]. Papers giving practical advise for the design of cells for NMR studies [17] and the separation of resonances from the different components of the cell [18] demonstrate the utility of this method.

In both CWGSR and $LiFePO_4$ battery, the active material is a porous medium. As seen in Fig. 1, in the CWGSR the primary particles are pressed into porous pellets, which are embedded in a fixed bed reactor. In the $LiFePO_4$ battery, primary particles form porous electrodes, which together with the electrolyte containing separator form a battery. In both cases, the challenge is to link the changes in magnetic susceptibility on the atomic level in the particle to the change in the effective susceptibility of the whole device, which is measurable from the outside. In this work, a hierarchical model for the magnetic permeability of a reactor with porous media was developed. This model describes the relationship of magnetic permeability and structure (particle size, porosity, etc.) of the device. The permeability model is general and applicable to chemical or electrochemical reactors with similar structure, like fixed bed or fluidized bed reactors, batteries, fuel cells or supercapacitors.

In the next section, the permeability model is described. Next, results for permeability of a $LiFePO_4$ battery as a function of the structure are discussed for both steady state and dynamic operation. Afterwards, the results for the CWGSR and the applicability of the method are discussed.

2 Hierarchical Model for Magnetic Permeability of a Porous Reactor

As shown in Fig.1, the model combines different scales: on the particle scale the model describes how the permeability of a single particle changes with oxidation state or SOC, respectively. On the porous medium scale, the permeability of the whole porous active medium (e.g. electrode or catalyst pellet) formed from single particles is described dependent on the porous structure (particle size, porosity etc.) of the medium. On the reactor scale both porous medium and passive components (e.g. separator and electrolyte in $LiFePO_4$ battery or gas flow field in CWGSR) are combined to determine the permeability of the whole reactor as function of oxidation state.

2.1 Particle Scale

In the following section, the effective magnetic susceptibility of a single particle's active material depending of its oxidation state is described. Three different scenarios for the distribution of the oxidized phase (i.e. distribution of lithium inside the particle in $LiFePO_4$ batteries, or the distribution of oxidized and unoxidized iron in CWGSR, respectively) are considered: First, uniform distribution of the oxidation state occurs, if intra-particle diffusion is negligible, e.g. because diffusion is faster than the reaction or intra-particle diffusion is fast compared to overall material transport in the reactor, e.g. because of the small diffusion length. This scenario is assumed for the positive carbon electrode of the $LiFePO_4$ battery and for the CWGSR particles.

The second scenario considers two distinct oxidation states in a core-shell like distribution. This can be the result of a phase separation (e.g. in $LiFePO_4$ batteries) or oxidation of the particle with a sharp reaction front. In the third scenario, a continuous distribution of the oxidation state in the particle is considered.

2.1.1 Particles with Uniform Oxidation State

As mentioned above, uniform distribution of the oxidation state is assumed in the CWGSR particles and on the positive carbon electrode in the $LiFePO_4$ battery. In the CWGSR, the diffusion length in the particle is small and the process is controlled by the reaction kinetics. In the $LiFePO_4$ battery, the diffusion coefficient of Li in carbon is 4 orders of magnitude larger than in $FePO_4$ [19]. Additionally, the particle size and with this the diffusion length is very small. Therefore, constant concentration of Li in carbon is assumed in steady state.

If the oxidized material (with permeability μ_h) is uniformly distributed in the host material (with permeability μ_o), the Maxwell-Garnet Approximation [20] can be used to estimate the effective permeability of the particle material [21, 22],

$$\frac{\mu_{pud}^{eff} - \mu_h}{\mu_{pud}^{eff} + (d-1)\mu_h} = p_o \frac{\mu_o - \mu_h}{\mu_o + (d-1)\mu_h}, \tag{1}$$

where d is the effective dimension or coordination number in which the problem is solved and p_o is the volume fraction of oxidized material.

In $LiFePO_4$ electrodes, p_o corresponds to the volume fraction of inter-

calated Li and is a function of the state-of-charge S. If the volume of the particles is assumed to be constant, it can be calculated according to

$$p_o = \frac{n_{Li} M_{Li}}{\rho_{Li} V_{pne}}, \quad (2)$$

$$n_{Li} = \frac{S \cdot C_{batt}}{ze}, \quad (3)$$

with the capacity of the battery C_{batt}, number of exchanged electrons z=1 and charge of an electron e.

2.1.2 Particles with Nonuniform Oxidation State

Two Distinct Oxidation States The $LiFePO_4$ electrode differs from intercalation electrodes in that it undergoes a phase change with the lithiated and unlithiated forms having distinct phases. This was found from X-ray diffraction (XRD) patterns of the material at various stages of lithiation [23, 24]. To describe this phase separation behavior, Srinivasan and Newman [19] developed a shrinking core model, which was incorporated into a general model framework of a lithium battery [25] and has been experimentally validated in half-cell experiments [19] and full cell experiments using a natural graphite/$LiFePO_4$ cell [26]

In order to determine the effective permeability of such a core-shell structured particle, a coated sphere model [21] can be used. For this model, exact results of the effective permeability are possible,

$$\mu_{pcs}^{eff} = \langle \mu \rangle - \frac{(\mu_c - \mu_s)\, p_c p_s}{\langle \tilde{\mu} \rangle + (d-1)\mu_s}, \quad (4)$$

with

$$\langle \mu \rangle = \mu_s p_s + \mu_c p_c, \tag{5}$$

$$\langle \tilde{\mu} \rangle = \mu_s p_c + \mu_c p_s, \tag{6}$$

where μ_s and p_s are the permeability and volume fraction of the shell and μ_c and p_c are the permeability and volume fraction of the core. In case of discharge of a fully charge electrode, lithium is inserted into a $FePO_4$ particle, thus s=$LiFePO_4$ and c=$FePO_4$. In case of charging a fully discharged electrode, $LiFePO_4$ particles are depleted of lithium, thus s=$FePO_4$ and c=$LiFePO_4$, i.e. the phases are reversed.

The volume fraction of $LiFePO_4$, p_{LiF}, is a function of the amount of inserted lithium and thus of the state-of-charge S. If the volume of the particles is assumed to be constant during intercalation (a valid assumption according to [19]), the volume fractions can be calculated according to

$$p_{LiF} = \frac{n_{LiF} M_{LiF}}{\rho_{LiF} V_{ppe}}, \tag{7}$$

$$n_{LiF} = n_{Li} = \frac{S \cdot C_{batt}}{ze}, \tag{8}$$

$$p_F = 1 - p_{LiF}. \tag{9}$$

Oxidation State Gradient In this work, continuous oxidation state gradients in the primary particles are not considered. Therefore, the approach shall only be described briefly. The determination of the oxidation state distribution in the primary particles (e.g. the distribution of Li in batteries) would require a more detailed reactor model that includes intra-particle transport, e.g. intra-particle diffusion in addition to the reaction occurring at the surface of the particle. Such transport model could be used to determine

the oxidation state (or Li concentration) as a function of radius of the particle. With this, each particle radius can be seen as an infinitesimally small shell with the determined oxidation state around a core with an effective permeability. In case the transport model is solved numerically, one would obtain a discrete number of small shells. Starting from the center of the particle, the infinitesimally small shells could be added in an iterative way and in each iteration the effective permeability is determined as described in the previous section. This iteration is repeated until the particle radius is reached, giving the effective permeability of the whole particle.

2.2 Porous Medium Scale

The porous medium (i.e. the porous electrodes in the $LiFePO_4$ battery or the catalyst pellets in the CWGSR) consists of primary particles, which are assumed to be electrically and thus magnetically connected to each other. Therefore, the differential effective medium approximation/Landau-Lifshitz-Looyenga (LLL) rule [27] can be used [21, 22]. This approach starts from a homogeneous component and uses an iterative procedure. First, a small amount of the homogeneous component is replaced by the second component. Then, the resulting "effective" material is regarded as the homogeneous component for the succeeding substitution step.

The LLL rule is obtained when the starting homogeneous material is the bulk medium of inclusions. If the starting material is the host matrix, the resulting equation is referred to as the differential EMT, or asymmetric Bruggeman approximation [28]. The LLL equation is rigorous when the

difference between the permeability of inclusions and that of the host matrix is small. It is independent of the shape of particles.

The effective permeability of the porous medium, μ_{pm}^{eff}, obtained in this approximation is

$$\mu_{pm}^{eff} = \left(\mu_{pore} + p_{pp}\left((\mu_{pp}^{eff})^{1/3} - (\mu_{pore})^{1/3}\right)^3\right), \tag{10}$$

where μ_{pore} is the permeability of the pore space (i.e. the electrolyte in the porous electrodes of the $LiFePO_4$ battery or the gas phase in the pellets of the CWGSR), p_{pp} and μ_{pp}^{eff} are the volume fraction and effective permeability of the primary particles as obtained in Section 2.1. For the CWGSR and the positive electrode of the $LiFePO_4$ battery, Eq.1 is used and $\mu_{pp}^{eff} = \mu_{pud}^{eff}$. For the negative $LiFePO_4$ electrode of the battery, Eq. 4 is used and $\mu_{pp}^{eff} = \mu_{pcs}^{eff}$.

2.3 Reactor Scale

The battery is assumed to have a layered structure consisting of positive electrode, electrolyte and negative electrode. For the permeability of a layered structure, a rigorous solution exists [21]. In through-plane direction, the permeability is the harmonic average of the permeabilities of the layers,

$$\left\langle (\mu_{bat}^{eff})^{-1} \right\rangle^{-1} = \left(\frac{p_{pe}}{\mu_{pe}^{eff}} + \frac{p_{sep}}{\mu_{sep}^{eff}} + \frac{p_{ne}}{\mu_{ne}^{eff}}\right)^{-1}. \tag{11}$$

In in-plane direction, the permeability is the arithmetic average of the permeabilities of the layers,

$$\left\langle \mu_{bat}^{eff} \right\rangle = p_{pe}\mu_{pe}^{eff} + p_{sep}\mu_{sep}^{eff} + p_{ne}^{eff}\mu_{ne}^{eff}. \tag{12}$$

Thus, the permeability matrix becomes

$$\mu_{bat}^{eff} = \begin{pmatrix} \left\langle (\mu_{bat}^{eff})^{-1} \right\rangle^{-1} & 0 & 0 \\ 0 & \left\langle \mu_{bat}^{eff} \right\rangle & 0 \\ 0 & 0 & \left\langle \mu_{bat}^{eff} \right\rangle \end{pmatrix}. \tag{13}$$

In the CWGSR, the porous pellets are surrounded by the gas phase and again the LLL rule (Eq. 10) is used to determine the permeability of the whole reactor bed:

$$\mu_{CWGSR}^{eff} = \left(\mu_{gas} + p_{pm} \left((\mu_{pm}^{eff})^{1/3} - (\mu_{gas})^{1/3} \right)^3 \right). \tag{14}$$

3 Results

The permeability model describes the permeability depending on the structure of the reactor. In the following, first the example of a $LiFePO_4$ battery is discussed in detail. At first, equilibrium conditions are considered. After that, the influence of nonuniform lithium distribution under dynamic operation conditions is discussed. Overall, the changes in magnetic susceptibility in a $LiFePO_4$ battery are small and challenging to measure. However, the results for the cyclic water gas shift reactor demonstrate a practically relevant example, in which the method can be easily applied.

Note that for convenience, instead of permeabilities the figures show susceptibilities ($\chi = 1 - \mu$).

3.1 $LiFePO_4$ Battery: Particle and Electrode Scales

3.1.1 Carbon Particles and Negative Electrode

In Fig. 2a, the black curve shows the magnetic susceptibility of the graphite particles for different lithium content. Since the lithium distribution in the particle is assumed to be uniform (the diffusion coefficient of Li in graphite is 4 orders of magnitude larger than in $FePO_4$ [26]), the susceptibility increases linearly with lithium content and thus with the state-of-charge. Pure graphite is slightly diamagnetic, i.e. its susceptibility is negative, and thus the insertion of paramagnetic lithium with positive susceptibility leads to the increase of the effective susceptibility of the particles.

The grey curve in Fig. 2a shows the effective susceptibility of the negative electrode taking the pores filled with electrolyte into account. The effective susceptibility of the electrode is an average of the constant susceptibility of the electrolyte and the changing susceptibility of the graphite particles. Thus, the qualitative behavior of the electrode is determined by the behavior of the graphite particles.

3.1.2 $LiFePO_4$ Particles and Positive Electrode

In Fig. 2b, the susceptibility of Li_xFePO_4 material as a function of lithium content x is shown in the black curve. The intercalated lithium changes the magnetic spin of the iron ions, which change from Fe^{3+} with spin S=5/2 to Fe^{2+} with S=2 [29]. If the magnetic spins and thus the lithium are homogeneously distributed, the susceptibility changes linearly, as shown in the black dashed line in Fig. 2b. This behavior is comparable to the case of the graphite

in the negative electrode, as described in the previous section. However, the susceptibility change of the $LiFePO_4$ with lithium content is 2 orders of magnitude larger than for graphite due to the interaction of lithium with the iron ions. This difference between the electrodes leads to a net change in the overall susceptibility of the battery.

However, as described in Section 2.1.2 lithium is not distributed uniformly inside the particles because phase separation occurs. Srinivasan [19] suggested that during discharge the lithium is first incorporated into a Li-rich shell around a Li-deficient core that shrinks upon lithium insertion. If all lithium is assumed to be within a $LiFePO_4$ shell around a $FePO_4$ core (which would correspond to a perfect phase separation), the susceptibility of the particle behaves as depicted by the upper black curve in Fig. 2b, i.e. a slight nonlinearity occurs. On the other hand, if the electrode is charged from a fully discharged state, the Li-enriched particles are depleted from lithium, thus they have a core of $LiFePO_4$ with a shell of $FePO_4$ surrounding them, i.e. the phases are reversed relative to the case of discharge. This leads to a different behavior in the case of charging, as shown with the lower black curve in Fig. 2b. Thus, a hysteresis occurs, which is caused by the core-shell structure.

The effective susceptibility of the positive electrode taking into account the electrolyte-filled pores is shown by the grey curves in Fig. 2b. As in the case of the negative electrode, the porosity does not change the behavior qualitatively, i.e. the susceptibility of the electrode is determined by the susceptibility of the $LiFePO_4$ particles.

3.2 Battery Scale

Fig. 3 shows the net susceptibility of the complete battery. The net susceptibility in through-plane direction is the harmonic average of the electrodes and the separator susceptibilities. The susceptibility of the separator is constant and the susceptibility of the negative graphite electrode is two orders of magnitude lower than that of the positive electrode (compare axes of Figs. 2a and b).

With this, the susceptibility is determined mainly by the susceptibility of the material Li_xFePO_4, i.e. by the change of the magnetic moment of the iron ions, and by the distribution of the lithium in the particle, i.e. the core-shell structure, which gives rise to a hysteresis.

Due to this hysteresis the magnetic permeability of the electrode does not depend on the SOC alone but also on the history of the electrode. Since in praxis the history of the electrode is often unknown, the determination of the SOC from the magnetic susceptibility alone would result in a significant uncertainty. For example, let us assume we would measure a susceptibility of $0.9{\cdot}10^{-4}$. According to Fig. 3, under slow charging conditions the SOC would be between 0.55 (charging from a completely discharged battery) and 0.7 (discharging from a completely charged battery), i.e. the uncertainty would be up to 12%.

A second important practical note is that the overall change in susceptibility is very small. This makes it very challenging to measure these changes. Very sensitive instrumentation with high signal to noise ratios would be required. Together with the uncertainty due to hysteresis, this makes the

practical applicability of this principle for $LiFePO_4$ batteries questionable.

3.2.1 Nonuniform Lithium Distribution in the Electrodes

The results in the previous section describe the permeability under equilibrium conditions, i.e. when lithium is uniformly distributed through the electrode. However, during charging and discharging, the lithium distribution in the electrodes can become nonuniform due to limited ion transport through the pores. Particles that are closer to the separator have shorter ion transport pathways and thus a higher local lithium concentration and charging rate. This effect is pronounced under fast charging conditions. In order to analyze the effect of the lithium distribution on the magnetic permeability, a porous transport model presented in Appendix B was used to determine the lithium distribution under different charging conditions. Using these lithium distributions, the magnetic permeability model was solved to determine the magnetic permeability of the battery under different charging conditions.

The influence of the lithium distribution on the magnetic susceptibility of the battery is shown in Fig. 3. For the case of a fully charged and fully discharged electrode, the lithium distribution is uniform, i.e. the electrode fully consists of either $LiFePO_4$ or $FePO_4$ particles. Thus, the lithium distribution has the biggest influence in the half-charged state. In this case, a more nonuniform Li distribution leads to a decrease of the hysteresis effect discussed in Section 3.1.2. As seen in Fig. 3, with increasing charge/discharge rate, the hysteresis disappears. A high charge/discharge rate leads to a more nonuniform lithium distribution. This results in part of the electrode being fully oxidized while another part of the electrode is fully reduced. Only

a small reaction zone contains partially oxidized particles with a core-shell structure. In the fully oxidized and fully reduced parts of the electrode there is no core-shell structure of the particles and thus these parts of the electrode do not contribute to the hysteresis. Only the core-shell particles in the reaction zone determine the hysteresis. Since the reaction zone becomes narrower with higher charge/discharge rate, the portion of the electrode that has a core-shell structure diminishes and the hysteresis decreases.

3.3 Cyclic Water Gas Shift Reactor

The magnetic susceptibility of a CWGSR catalyst particle, porous pellet and reactor bed are shown in Fig. 4. It can be seen that the primary particles undergo a significant change in magnetic susceptibility during oxidation. This change is 4 orders of magnitude larger than in the case of $LiFePO_4$ battery described before and should be easy to measure practically. Additionally, no phase separation and thus no hysteresis occurs.

Qualitatively, the change in susceptibility with oxidation state is non-linear. Upon oxidation, first a large drop in susceptibility occurs. After the particle is about 20% oxidized, the susceptibility continues to decrease approximately linearly. The same qualitative trend follows in the catalyst pellets and finally in the whole reactor bed. The overall change in susceptibility is about 149 on the particle scale; it drops to to 34 and 2 on the porous medium and reactor scale, respectively.

4 Summary and Conclusions

In this work, the possibility of using the magnetic susceptibility as a direct measure of the oxidation state of a reactor with porous active material was investigated. Two specific examples were selected: a $LiFePO_4$ battery and a cyclic water gas shift reactor. In $LiFePO_4$ batteries, the intercalation of lithium in the negative electrode changes the oxidation state of the iron atoms; therefore the oxidation state can indicate the state-of-charge. In the cyclic water gas shift reactor, the active material acts as an oxygen storage for the reaction and the oxidation state corresponds to the oxygen level of this storage.

In order to determine the change of the magnetic susceptibility with SOC or oxygen storage level, a multiscale model was used which describes the relationship between magnetic permeability and structure (particle size, porosity, lithium distribution etc.) of the reactor. In the $LiFePO_4$ battery, it was found that the change in the susceptibility of the $LiFePO_4$ particles on the atomic scale of the positive electrode has the largest influence on the net change of the susceptibility of the battery.

Additionally, in the particles a phase separation between lithiated and non-lithiated $FePO_4$ occurs, which leads to a core-shell structure. The history of the electrode, i.e. whether it was charged from an uncharged state or discharged from a charged state, determines, which phase is in the core and which is in the shell. After charging, the shell consists of $LiFePO_4$ around a $FePO_4$ core, after discharging there is a $FePO_4$ shell around a $LiFePO_4$ core. This phase inversion leads to a different magnetic permeability depending

on the history of the electrode, i.e. hysteresis occurs. The limiting cases for this hysteresis, namely charging from a completely discharged state and discharging from a completely charged state, were analysed.

The permeability model was coupled with an electrochemical model of a $LiPePO_4$ electrode in order to investigate the influence of the lithium distribution in through plane direction of the electrode. Thus, the electrochemical model gives structural information depending on the operation (current density, charging time etc.) of the battery which can be used as input parameters for the permeability model.

The electrochemical model revealed the occurrence of moving reaction zones during fast charge or discharge. This reaction zone behavior leads to a decrease of the magnetic hysteresis effect because with a narrow reaction zone at high current densities only a small part of the electrode has a core-shell structure. The rest of the electrode consists of either fully oxidized or fully reduced particles which do not contribute to a hysteresis.

The model is thus insightful in terms of understanding the basic relation between magnetic properties and electrochemical processes of a battery. Practical applicability as a diagnostic method to determine the SOC is however limited. For $LiFePO_4$ electrodes the sensitivity of the magnetic response to SOC lies in the range of $\sim 0.03\%$ - this would require a signal-to-noise ratio of $\sim$ 90dB. For other materials this requirement is expected to be significantly smaller. Additionally, the permeability depends not only on SOC but also on the history of the electrode, which is usually unknown. Thus, the discussed hysteresis leads to a high uncertainty in the determination of the SOC.

However, in cyclic water gas shift reactors, the change of susceptibility was found to be orders of magnitude larger, which allows for easy measurement. Additionally, no phase separation and thus no magnetic hysteresis occurs. This example shows that in cases, in which large changes of the magnetic nature of the active material occur, e.g. transition from ferromagnetic to paramagnetic behavior, the measurement of the magnetic susceptibility might provide insightful information about the state of the reactor.

5 Acknowledgements

We appreciate the discussions with the staff of Cadex Electronics Inc. and especially Joe Geofroy and Delaram Abdollazadeh and their experimental trials. Furthermore we are thankful for the financial support from the NSERC Engage Grants program.

References

[1] Charles Kittel. *Introduction to Solid State Physics*. John Wiley & Sons, 1986.

[2] P. Heidebrecht, C. Hertel, and K. Sundmacher. Conceptual analysis of a cyclic water gas shift reactor. *International Journal of Chemical Reactor Engineering*, 6:A19, 2008.

[3] P. Heidebrecht and K. Sundmacher. Thermodynamic analysis of a cyclic water gas-shift reactor (CWGSR) for hydrogen production. *Chemical Engineering Science*, 64(23):5057–5065, December 2009.

[4] C. Hertel, P. Heidebrecht, and K. Sundmacher. Experimental quantification and modelling of reaction zones in a cyclic watergas shift reactor. *International Journal of Hydrogen Energy*, 37(3):2195–2203, February 2012.

[5] S. Piller, M. Perrin, and A. Jossen. Methods for state-of-charge determination and their applications. *Journal of Power Sources*, 96(1):113–120, June 2001.

[6] V. Pop, H. J. Bergveld, P. H. L. Notten, and P. P. L. Regtien. State-of-the-art of battery state-of-charge determination. *Measurement Science & Technology*, 16(12):R93–R110, December 2005.

[7] J. Vetter, P. Novak, M. R. Wagner, C. Veit, K. C. Moller, J. O. Besenhard, M. Winter, M. Wohlfahrt-Mehrens, C. Vogler, and A. Hammouche. Ageing mechanisms in lithium-ion batteries. *Journal of Power Sources*, 147(1-2):269–281, September 2005.

[8] E. Bekaert, P. Balaya, S. Murugavel, J. Maier, and M. Menetrier. Li-6 MAS NMR investigation of electrochemical lithiation of RuO_2: Evidence for an interfacial storage mechanism. *Chemistry of Materials*, 21(5):856–861, March 2009.

[9] J. H. Trill, C. Q. Tao, M. Winter, S. Passerini, and H. Eckert. NMR investigations on the lithiation and delithiation of nanosilicon-based anodes for Li-ion batteries. *Journal of Solid State Electrochemistry*, 15(2):349–356, February 2011.

[10] K. Gotoh, M. Maeda, A. Nagai, A. Goto, M. Tansho, K. Hashi, T. Shimizu, and H. Ishida. Properties of a novel hard-carbon optimized to large size li ion secondary battery studied by Li-7 NMR. *Journal of Power Sources*, 162(2):1322–1328, November 2006.

[11] H. Fujimoto, A. Mabuchi, K. Tokumitsu, N. Chinnasamy, and T. Kasuh. (7)Li nuclear magnetic resonance studies of hard carbon and graphite/hard carbon anode for Li ion battery. *Journal of Power Sources*, 196(3):1365–1370, February 2011.

[12] H. Hain, M. Scheuermann, R. Heinzmann, L. Wunsche, H. Hahn, and S. Indris. Study of local structure and Li dynamics in Li_4+xTi_5O_{12} (0 <= x <= 5) using Li-6 and Li-7 NMR spectroscopy. *Solid State Nuclear Magnetic Resonance*, 42:9–16, April 2012.

[13] S. Chandrashekar, N. M. Trease, H. J. Chang, L. S. Du, C. P. Grey, and A. Jerschow. Li-7 MRI of Li batteries reveals location of microstructural lithium. *Nature Materials*, 11(4):311–315, April 2012.

[14] L. J. M. Davis, B. L. Ellis, T. N. Ramesh, L. F. Nazar, A. D. Bain, and G. R. Goward. Li-6 1D EXSY NMR spectroscopy: A new tool for studying lithium dynamics in paramagnetic materials applied to monoclinic Li_2VPO_4F. *Journal of Physical Chemistry C*, 115(45):22603–22608, November 2011.

[15] R. Bhattacharyya, B. Key, H. L. Chen, A. S. Best, A. F. Hollenkamp, and C. P. Grey. In situ NMR observation of the formation of metallic

lithium microstructures in lithium batteries. *Nature Materials*, 9(6):504–510, June 2010.

[16] J. Xiao, J. Z. Hu, D. Y. Wang, D. H. Hu, W. Xu, G. L. Graff, Z. M. Nie, J. Liu, and J. G. Zhang. Investigation of the rechargeability of Li-O_2 batteries in non-aqueous electrolyte. *Journal of Power Sources*, 196(13):5674–5678, July 2011.

[17] F. Poli, J. S. Kshetrimayum, L. Monconduit, and M. Letellier. New cell design for in-situ NMR studies of lithium-ion batteries. *Electrochemistry Communications*, 13(12):1293–1295, December 2011.

[18] N. M. Trease, L. N. Zhou, H. J. Chang, B. Y. X. Zhu, and C. P. Grey. In situ NMR of lithium ion batteries: Bulk susceptibility effects and practical considerations. *Solid State Nuclear Magnetic Resonance*, 42:62–70, April 2012.

[19] Venkat Srinivasan and John Newman. Discharge model for the lithium iron-phosphate electrode. *Journal of The Electrochemical Society*, 151(10):A1517, 2004.

[20] J. C. Maxwell Garnett. Colours in metal glasses and in metallic films. *Philosophical Transactions of the Royal Society A*, 203:385 – 420, 1904.

[21] S. Torquato. *Random Heterogeneous Materials – Microstructure and Macroscopic Properties*. Springer, 2002.

[22] Andrey N. Lagarkov and Konstantin N. Rozanov. High-frequency behavior of magnetic composites. *Journal of Magnetism and Magnetic Materials*, 321(14):2082–2092, July 2009.

[23] A. K. Padhi, K. S. Nanjundaswamy, and J. B. Goodenough. Phospho-olivines as positive-electrode materials for rechargeable lithium batteries. *Journal of the Electrochemical Society*, 144(4):1188–1194, April 1997.

[24] A. Yamada, Y. Kudo, and K. Y. Liu. Phase diagram of $\mathrm{Li}_x(\mathrm{Mn}_y\mathrm{Fe}_{(1-y)}\mathrm{PO}_4$ (0 <= x, y <= 1). *Journal of the Electrochemical Society*, 148(10):A1153–A1158, October 2001.

[25] K. E. Thomas, J. Newman, and R. M. Darling. *Advances in Lithium-Ion Batteries*, chapter 12, pages 345–392. Kluwer Academic Publishers, 2002.

[26] Venkat Srinivasan and John Newman. Design and optimization of a natural graphite/iron phosphate lithium-ion cell. *Journal of The Electrochemical Society*, 151(10):A1530, 2004.

[27] L. Landau and E. Lifshitz. *Electrodynamics of Continuous Media*. Pergamon Press, Oxford, 1960.

[28] D. A. G. Bruggeman. Berechnung verschiedener physikalischer Konstanten von heterogenen Substanzen. *Annalen der Physik*, 24:636 – 679, 1935.

[29] P. Jozwiak, J. Garbarczyk, F. Gendron, A. Mauger, and C. M. Julien. Disorder in Li_xFePO_4: From glasses to nanocrystallites. *Journal of Non-crystalline Solids*, 354(17):1915–1925, April 2008.

[30] C. S. Wang and J. Hong. Ionic/electronic conducting characteristics of $LiFePO_4$ cathode materials - The determining factors for high rate performance. *Electrochemical and Solid State Letters*, 10(3):A65–A69, 2007.

[31] N. Ravet, J. B. Goodenough, S. Besner, M. Simoneau, P. Hovington, and M. Armand. In *The Electrochemical Society and the Electrochemical Society of Japan Meeting Abstracts, Vol. 99–22, Honululu, HI*, 1999.

[32] S. Y. Chung, J. T. Bloking, and Y. M. Chiang. Electronically conductive phospho-olivines as lithium storage electrodes. *Nature Materials*, 1(2):123–128, October 2002.

[33] P. S. Herle, B. Ellis, N. Coombs, and L. F. Nazar. Nano-network electronic conduction in iron and nickel olivine phosphates. *Nature Materials*, 3(3):147–152, March 2004.

[34] C. Lin, J. A. Ritter, B. N. Popov, and R. E. White. A mathematical model of an electrochemical capacitor with double-layer and faradaic processes. *Journal of the Electrochemical Society*, 146(9):3168–3175, September 1999.

A Magnetic Permeability of $LiFePO_4$ and delithiated $FePO_4$

The permeability of $LiFePO_4$ and delithiated $FePO_4$ can be determined from the effective magnetic moment. According to [29], the experimental magnetic moment for Li_xFePO_4 ($0 \leq x \leq 1$) is in good agreement with the theoretical spin-only values for Fe^{3+} and Fe^{2+},

$$\mu_{eff}^{theor} = \mu_B \sqrt{x p_{Fe^{2+}}^2 + (1-x) p_{Fe^{3+}}^2}. \tag{15}$$

The effective number of Bohr magnetons p is expected to correspond to the spin-only theoretical value according to

$$p = 2\left[S(S+1)\right]^{1/2}, \tag{16}$$

where S=2 for Fe^{2+} in $LiFePO_4$ and S=5/2 for Fe^{3+}.

The effective magnetic moment μ_{eff} is related to the Curie constant C_p,

$$C_p = \frac{N_A \mu_{eff}{}^2}{3k_B}, \tag{17}$$

with Boltzmann constant k_B and Avogadro's number N_A. The molar magnetic susceptibility χ_m can then be derived from the Curie-Weiss law,

$$\chi_m = \frac{C_p}{T - \theta_p}, \tag{18}$$

which is valid in the paramagnetic regime at temperatures above the Curie temperature $T > T_C \sim 100K$ [29].

B Dynamic Battery Model

The permeability model can describe the permeability as function of SOC in the case of uniform lithium distribution in the electrode. This assumption is valid under equilibrium conditions. However, under dynamic conditions the lithium distribution has to be taken into account. In this section, an electrochemical model of the positive electrode is developed that describes the lithium distribution dynamically during battery operation. The model includes the double layer, electrochemical reaction, ion transport in the porous electrode and electron transport in the solid phase. Lithium transport into the particle and the core-shell structure of the Li_xFePO_4 particles are described in a simplified way. Afterwards, the resulting lithium distribution is coupled into the permeability model. Thus, the permeability of the battery under dynamic conditions can be analysed.

B.1 Basic Model Equations

In the following, the reaction scheme of the model is explained. Charge balance equations for the electron and ion conducting phases and the electrochemical double layer are given. A kinetic equation for the reaction is given. Lithium transport into the particles is described based on a simplified shrinking core model.

At the surface of the particles, the following reaction occurs:

$$LiFePO_4 \underset{discharge}{\overset{charge}{\rightleftharpoons}} FePO4 + Li^+ + e^- \tag{19}$$

The charge balance in the electrolyte phase can be described under the assumption of electroneutrality as

$$0 = -\frac{\partial}{\partial z}\underbrace{\left(-\kappa_l^{eff}\frac{\partial \phi_l}{\partial z}\right)}_{i_l} + a \cdot \iota, \tag{20}$$

where ϕ_l is the potential in the electrolyte, κ_l^{eff} is the effective conductivity of the electrolyte, ι is the charge flux and a is the specific active surface area.

The boundary conditions to solve Eq.20 under galvanostatic or potentiostatic operation are

$$\left.\frac{\partial \phi_l}{\partial z}\right|_{z=0} = 0 \qquad \forall\, t \tag{21}$$

$$-\kappa_l^{eff}\left.\frac{\partial \phi_l}{\partial z}\right|_{z=L} = i_{cell}\,(t) \qquad \forall\, t \qquad \text{(galvanostatic)} \tag{22}$$

$$\phi_l\,(z = L, t) = \phi_{sep,a}\,(t) \qquad \forall\, t \qquad \text{(potentiostatic)} \tag{23}$$

where i_{cell} is the current density per geometric area and $\phi_{sep,a}$ is the electrode potential at the electrode-separator interface, i.e. the cell voltage minus the overpotentials of negative electrode and separator.

The potential distribution in the solid, electron conducting phase under

the assumption of electroneutrality is given by

$$0 = -\frac{\partial}{\partial z}\underbrace{\left(-\kappa_s^{eff}\frac{\partial \phi_s}{\partial z}\right)}_{i_s} + a \cdot \iota \tag{24}$$

The boundary conditions for the electron conducting phase are

$$\left.\frac{\partial \phi_s}{\partial z}\right|_{z=L} = 0 \qquad \forall\, t \tag{25}$$

$$\phi_s\left(z=0,t\right) = 0 \qquad \forall\, t \tag{26}$$

The charge balance for the double layer is given as

$$C_{dl}\frac{\partial \Delta\phi}{\partial t} = \iota - F r^{ox} \tag{27}$$

with

$$\Delta\phi = \phi_s - \phi_l \tag{28}$$

$$\eta = \Delta\phi - \Delta\phi^{0,ref} \tag{29}$$

where η is the overpotential of the positive electrode and C_{dl} is the double layer capacity. The oxidation rate, r^{ox}, in Eq.27 is dependent on the concentration of lithium in the solid lattice at the particle surface, c_s:

$$r^{ox} = k^{ox}\left(\frac{c_s}{c_{ref}}\exp\left(\frac{\alpha n F}{RT}\eta\right) - \exp\left(-\frac{\left(1-\alpha\right)nF}{RT}\eta\right)\right) \tag{30}$$

In order to determine the surface concentration c_s of lithium in the solid, usually lithium transport into the solid phase is evaluated. However, the $LiFePO_4$ electrode differs from intercalation electrodes in that a phase sep-

aration between the lithiated and unlithiated Li_xFePO_4 phases occurs, as found from XRD studies [23, 24]. To model this behavior, Srinivasan and Newman [19] developed a shrinking core model, which was incorporated into a general model framework of a lithium battery [25] and has been experimentally validated in half-cell experiments [19] and full cell experiments using a natural graphite/$LiFePO_4$ cell [26].

In this work, we use a simplified approach to describe the shrinking core behavior. It is assumed that all lithium in the particle is in a single $LiFePO_4$ phase (in the core during charging, when Li is removed from the particle or in the shell during discharge, when Li is incorporated). The rest of the particle consists of a $FePO_4$ phase and both phases are perfectly separated from each other. In this case, the surface of the particle consists either of $FePO_4$ during charge or of $LiFePO_4$ during discharge. The reaction rate is independent of surface concentration in the solid but different reaction rate constants for charge and discharge are possible. This can be described as

$$r^{ox} = \tilde{k}^{ox}\left(\exp\left(\frac{\alpha nF}{RT}\eta\right) - \exp\left(-\frac{(1-\alpha)\,nF}{RT}\eta\right)\right), \tag{31}$$

with

$$\tilde{k}^{ox} = \tilde{k}^{ox}_{ch} \quad (charging), \tag{32}$$

$$\tilde{k}^{ox} = \tilde{k}^{ox}_{dch} \quad (discharging). \tag{33}$$

The amount of lithium in the particle, n_{Li}, is given by

$$n_{Li} = \int_0^t r^{ox} dt. \tag{34}$$

If the amount of lithium reaches the maximum amount that can be stored

in the electrode, the reaction rate drops to zero,

$$r^{ox} = 0 \quad \text{for} \quad n_{Li} \geq n_{Li}^{max}. \tag{35}$$

Thus, the concentration dependency of the reaction rate is approximated by a step function.

The model was solved using the parameters in Table 1.

B.2 Results and Discussion

B.2.1 Limited Electron Conductivity

$LiFePO_4$ has the disadvantage of poor rate performance due to its low electron conductivity ($\sim 10^{-9}$ S/m) [30]. Several methods are used to enhance electron conductivity: carbon coating [31], ion doping [32] or nano networking [33]. However, in the works of Srinivasan et al. with carbon coated particles, the electron conductivity was determined to be about 10 times lower than the electrolyte conductivity. If the electron conductivity is that low and the battery is discharged rapidly, the distribution of lithium content and reaction rate evolves as depicted in Fig. 5. The limited electron conduction from the current collector side into the electrode leads to a reduction of the electrode at the current collector side (z=0) first. After the material in this "reaction zone" is reduced, the reaction zone moves further toward the separator side. This results in a moving reaction zone. With this, lithium is inserted from the current collector side towards the separator side of the electrode.

B.2.2 Limited Electrolyte Conductivity

If the electron conductivity could be significantly increased, the electrolyte conductivity becomes the limiting factor during rapid discharge. The distribution of lithium content and reaction rate for this scenario are shown in Fig. 6. Due to the limited ion transport from the separator into the electrode, the electrode is reduced in a small reaction zone at the separator-electrode interface first. When the material in this zone is reduced, the reaction zone moves into the electrode. Correspondingly, lithium is inserted into the electrode from the separator towards the current collector side.

B.2.3 Limited Electrolyte and Electron Conductivity

If electron and ion conductivity are equally limited, both moving reaction zones can occur simultaneously, as shown in Fig. 7. Starting from separator and current collector side, the electrode is reduced towards the inside of the electrode. Thus, lithium is inserted in the inside part of the electrode last.

Please note that the reaction rate profiles in Fig. 5-7b show the drop of the reaction rate when the material is fully reduced as a step function. This results in a spike shape of the maximum reaction rate. These features are caused by the simplifications made in Section B.1. Nevertheless, the model is able to capture the main phenomena during electrode operation.

B.3 Connecting Battery and Permeability Model

Solving the battery model gives the lithium distribution across the electrode, $n_{Li}(z)$. Each position z can be seen as an infinitely small layer with a perme-

ability that can be determined according to Sections 2.1.2 and 2.2. Thus, the permeability distribution across the electrode, $\mu(z)$ is obtained. The effective permeability across the whole electrode can then be calculated according to the permeability of a layered structure, i.e. by calculating the harmonic average of the layers:

$$\mu_{pe}^{eff} = \frac{1}{\int \frac{z}{\mu_{ppe}(z)} dz}. \tag{36}$$

With this, the permeability of the battery can be calculated according to Section 2.3.

Table 1: Model Parameters

	used value	reference
C_{dl}	0.2 F m_{act}^{-2}	[34]
d	52^{-9} m	[19]
$k_{RuO_2}^{ox}$	$5.15{\cdot}10^{-15}$ mol s^{-1} m_{act}^{-2}	[26]
	from i_0=3.14^{-6} A cm^{-2}	
L	$75{\cdot}10^{-6}$	[19]
T	298 K	assumed
α	0.5	[19]
ϵ	0.27	[19]
κ_l^{eff}	$4.03{\cdot}10^{-2}$ S m^{-1}	[19]
κ_s^{eff}	$5{\cdot}10^{-3}$ S m^{-1}	[19]

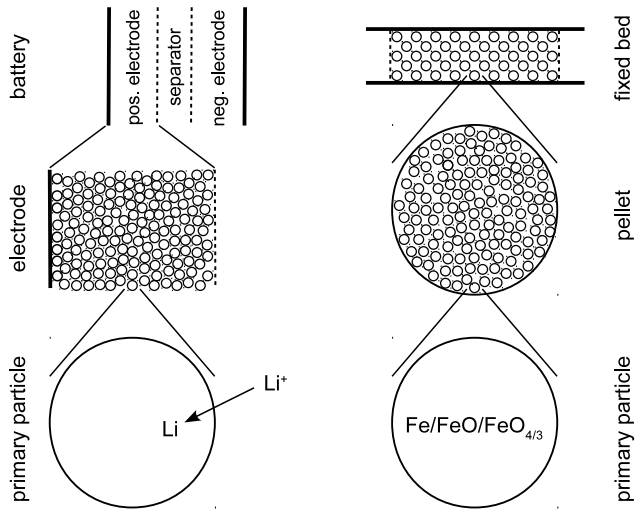

Figure 1: Schematic representation of the three structural scales of a $LiFEPO_4$ battery (left) and a cyclic water gas shift reactor (right).

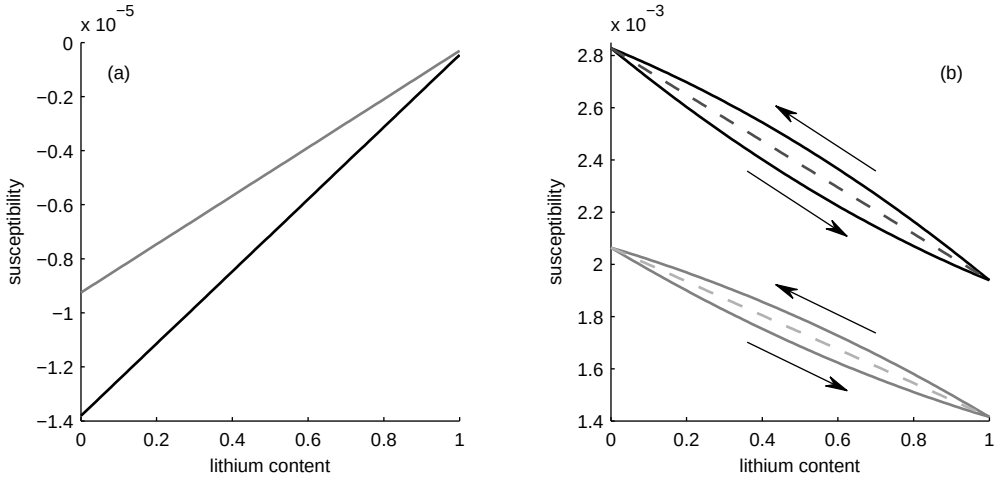

Figure 2: Susceptibility as function of lithium content. (a) Negative electrode: bulk material (black) and porous electrode structure (grey). (b) Positive electrode: bulk material (black), for homogeneous lithium distribution in the porous electrode (dashed line) and using the core-shell model (solid line).

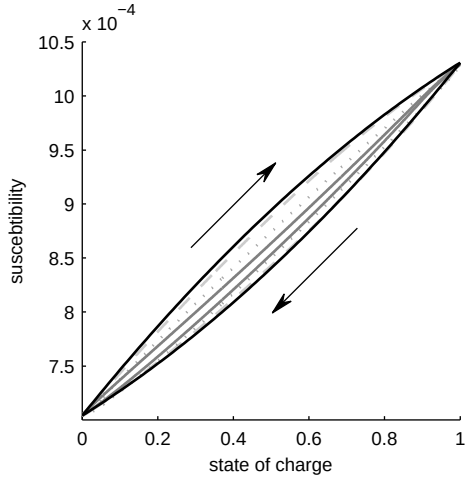

Figure 3: Susceptibility of a $LiFePO_4$ battery as function of SOC for different charge/discharge rates. Black line: infinitely slow discharge, dashed grey line: 1C (=1.2mA/cm^2), dotted line 10C (=12mA/cm^2), solid grey line: 100C(=124mA/cm^2).

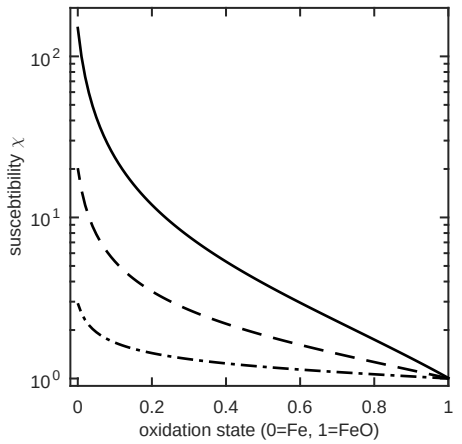

Figure 4: Susceptibility of a CWGSR particle (solid line), pellet (dashed line) and reactor bed (dotted line) as function of oxidation state

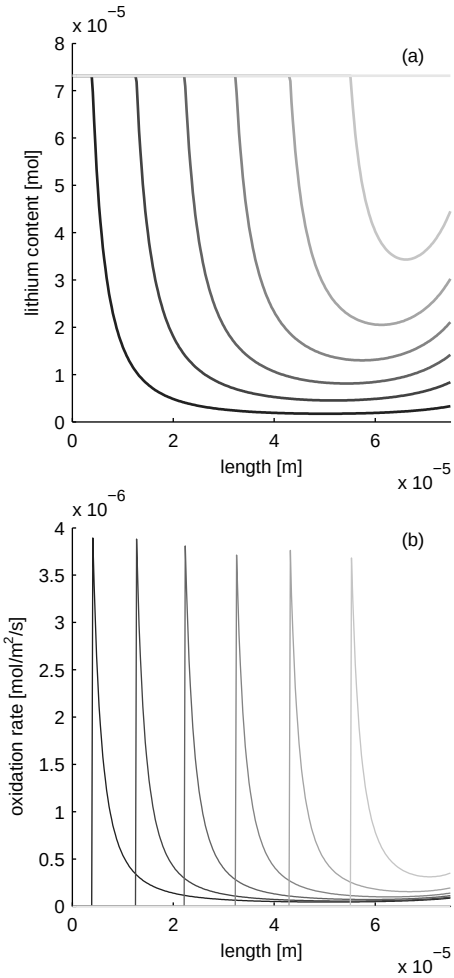

Figure 5: Moving reaction front in a $LiFePO_4$ electrode with low electron conductivity during fast charging with 10C (=12mA/cm^2). (a) lithium distribution and (b) reaction rate distribution at different times (from black to gray: 0, 0.39, 0.78, 1.17, 1.56, 1.95, 2.34 s).

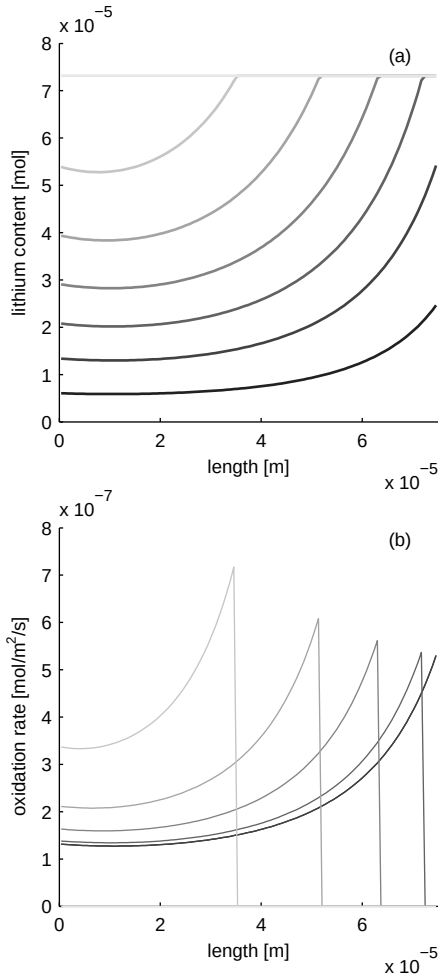

Figure 6: Moving reaction front in a $LiFePO_4$ electrode with high electron conductivity during fast charging with 10C (=12mA/cm^2). (a) lithium distribution and (b) reaction rate distribution at different times (from black to gray: 0, 0.39, 0.78, 1.17, 1.56, 1.95, 2.34 s).

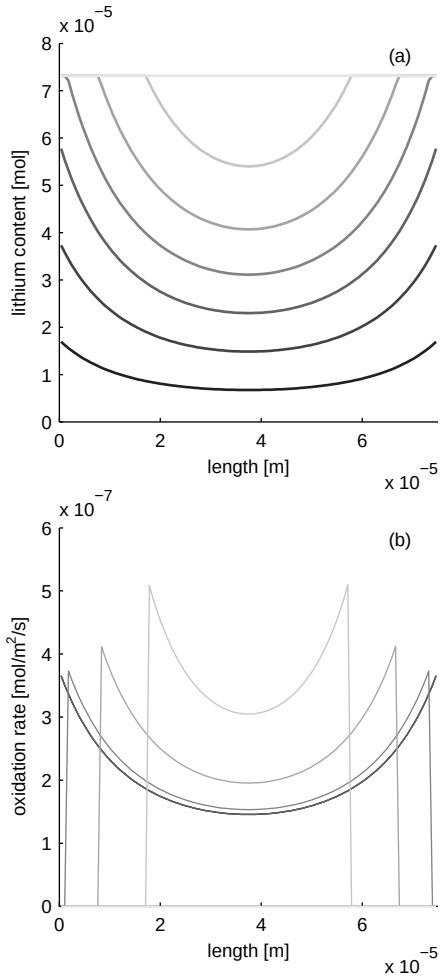

Figure 7: Moving reaction front in a $LiFePO_4$ electrode with equal electron and ion conductivity during fast charging with 10C (=12mA/cm^2). (a) lithium distribution and (b) reaction rate distribution at different times (from black to gray: 0, 0.39, 0.78, 1.17, 1.56, 1.95, 2.34 s).